IL NUOVO CIMENTO **42 C** (2019) 251
DOI 10.1393/ncc/i2019-19251-2

COLLOQUIA: La Thuile 2019

CP violation in charmless multi-body beauty decays

C. COSTA SOBRAL on behalf of the LHCb COLLABORATION
Department of Physics, University of Warwick - Coventry, UK

received 10 October 2019

Summary. — The multi-body charmless decays of beauty hadrons are rich in CP-violating phenomena. The LHCb experiment plays an important role in b-quark physics, with its ability to study all types of b-hadrons. This document outlines some of the latest results on multi-body charmless b-meson decays from the LHCb experiment. The first amplitude analyses of the decays $B_s^0 \to K_S^0 K^\pm \pi^\mp$ and the decay $B^\pm \to \pi^\pm K^+ K^-$ are presented.

1. – Introduction

An important goal of modern particle physics is understanding the matter-antimatter asymmetry in the universe. In the Standard Model (SM), the single source of CP violation is the complex phase of the Cabibbo-Kobayashi-Maskawa (CKM) mixing matrix [1, 2]. However, this only accounts for a small amount of the total observed asymmetry. The search for New Physics (NP) effects beyond the SM, which could introduce new sources of CP violation, is therefore an key area of research.

The presence of CP-violating effects in the beauty sector is well established. Furthermore, the charmless decays of b-hadrons have the potential to exhibit large CP-violating effects. The tree-level $b \to u$ transition has comparable magnitude to the loop-level $b \to s, d$ transitions, and the interference between them can provide both the weak and strong phase differences necessary for CP violation to emerge. For example, significant CP violation has been observed in the two-body decays of B^0 and B_s^0 to charged kaons and pions [3], and the decay $B^\pm \to \pi^\pm K^+ K^-$ [4].

Multi-body decays, such as $B^\pm \to \pi^\pm K^+ K^-$, are particularly of interest since the CP asymmetry $\mathcal{A}_{CP}$ can vary as a function of the phase space of the decay. In addition to the interference between tree and loop amplitudes, the different intermediate states that contribute to a particular final state can also interfere with each other, providing a different source of the strong phase difference required for CP violation. In fact, in $B^\pm \to \pi^\pm K^+ K^-$ and the related decays $B^\pm \to K^\pm K^+ K^-, K^\pm \pi^+ \pi^-, \pi^\pm \pi^+ \pi^-$, regions of the phase space with very large $\mathcal{A}_{CP}$ have been observed [4].

A crucial technique to study multi-body decays is the amplitude analysis, *i.e.* the modelling of the variation of the complex amplitude of a particular decay as a function

of its phase-space. This modelling is commonly carried out via the 'isobar model': the full decay amplitude is modelled as the coherent sum of a number of individual quasi-two-body decay amplitudes,

$$\mathcal{A}(m^2_{ij}, m^2_{jk}) = \sum_R c_R F_R(m^2_{ij}, m^2_{jk}), \tag{1}$$

where m_{ij}, m_{jk} are two-body invariant mass combinations of the three final-state particles (i, j, k) and, for each intermediate state R, F_R describes the dynamics of said state, and c_R describes its relative magnitude and phase. An equivalent amplitude $\bar{\mathcal{A}}$ can be constructed, in terms of $\bar{c}_R$ and $\bar{F}_R$, for the *CP*-conjugate state. The magnitude and phase of c_R and $\bar{c}_R$ can be extracted by fitting the model to data and used to construct quantities such as the fit fraction and $\mathcal{A}_{CP}$ of each intermediate state R.

2. – Amplitude analysis of $B^0_s \to K^0_S K^\pm \pi^\mp$ decays

The decays of the B^0_s meson are an interesting sector for the study of *CP* violation effects, via decay-time-dependent analyses of these decays. Measurements have been performed for two- and quasi-two-body B^0_s decays [3, 5], however there are no previous measurements for three-body B^0_s decays. The $B^0_s \to K^0_S K^\pm \pi^\mp$ decays have been previously observed [6, 7], with this analysis being the first amplitude analysis of these decays [8]. The modest tagging efficiency achieved at LHCb, coupled with small signal yields, requires this analysis to be performed in a decay-time-independent manner and without separation of the B^0_s and $\overline{B}^0_s$ initial states.

Both the $K^0_S\ K^+\ \pi^-$ and $K^0_S\ K^-\ \pi^+$ final states are accessible to the two initial states, with the two contributions to each final state expected to have similar magnitudes. The untagged approach taken in this analysis implies that the variation across the Dalitz plot (DP) of each final state must be described by a single amplitude, despite the fact that the physical amplitude is the incoherent sum of the B^0_s and $\overline{B}^0_s$ contributions. Pseudoexperiment studies show that fit fractions extracted with this approach are robust.

The event selection requirements for this analysis are based on, and follow closely, the requirements used in the previous determination of the branching fractions [7]. The data sample used is also the same, corresponding to $3.0\,\text{fb}^{-1}$ of data taken by the LHCb detector in 2011 and 2012. The reconstructed $K^0_S \to \pi^+\pi^-$ decays are classified based on whether the K^0_S meson is reconstructed from tracks with hits within the vertex locator, or tracks with hits downstream of the vertex locator only. These two K^0_S categories are referred to as *long* and *downstream*, respectively. There are roughly twice as many *downstream* K^0_S candidates, however *long* candidates have better vertexing and momentum resolution. The B^0_s candidates are also classified in this manner, based on the category of the associated K^0_S meson. Furthermore the data sample is subdivided into three data-taking periods, to account for differences in the K^0_S trigger efficiency.

A boosted decision tree (BDT) is trained on the topological features of the decays in order to supress background from random combinations of tracks, while particle identification (PID) is used to separate candidates into one of four final states: $K^0_S\ \pi^+\ \pi^-$, $K^0_S\ K^+\ \pi^-$, $K^0_S\ K^-\ \pi^+$, and $K^0_S\ K^+\ K^-$. Backgrounds proceeding via intermediate charmed and charmonium states are removed via a number of vetoes on the two-body invariant mass combinations of the final-state particles.

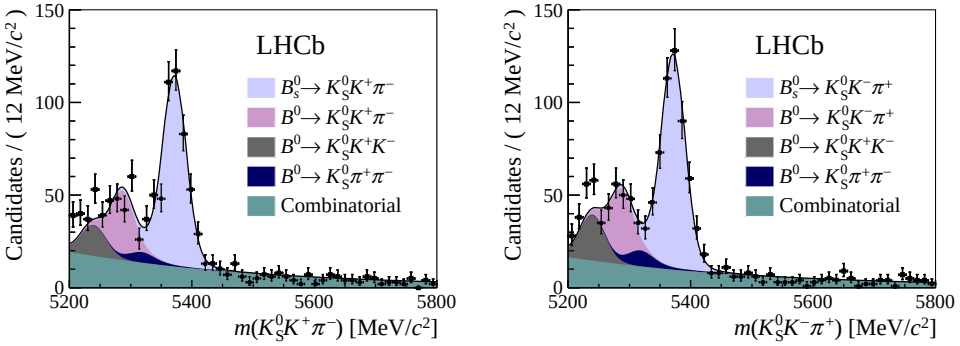

Fig. 1. – Invariant-mass distributions of the signal candidates for the $K^0_S\ K^+\ \pi^-$ (left) and $K^0_S\ K^-\ \pi^+$ (right) final states [8].

An unbinned extended maximum-likelihood fit is performed simultaneously to the 24 data sub-samples (four final states, three data-taking periods, and two K^0_S categories) in order to determine signal and background yields. Each contribution from signal and cross-feed from misidentified $B^0_{(s)} \to K^0_S h^+ h'^-$ is modelled using the sum of two Crystal Ball functions, with shared value for the peak position and width. The yields of the cross-feed backgrounds are constrained relative to the yields obtained in the spectra in which they are specifically selected as signal. The combinatorial background component is modelled using an exponential function. The fit results are shown for the two final states in fig. 1, with the six subsamples for each final state combined. Only candidates within a small region around the fitted peak position are used for the amplitude analysis. Within this region, defined as ± 2.5 times the fitted signal width, 529 signal candidates are selected for the $K^0_S\ K^+\ \pi^-$ final state and 573 signal candidates for the $K^0_S\ K^-\ \pi^+$ final state.

The Dalitz plot distributions, corrected for variations in the signal efficiency and with backgrounds subtracted, are shown in fig. 2. Visual evidence of resonant contributions at low values of both $m^2(K^0_S\pi^\mp)$ and $m^2(K^\pm\pi^\mp)$ can be seen, however no such struc-

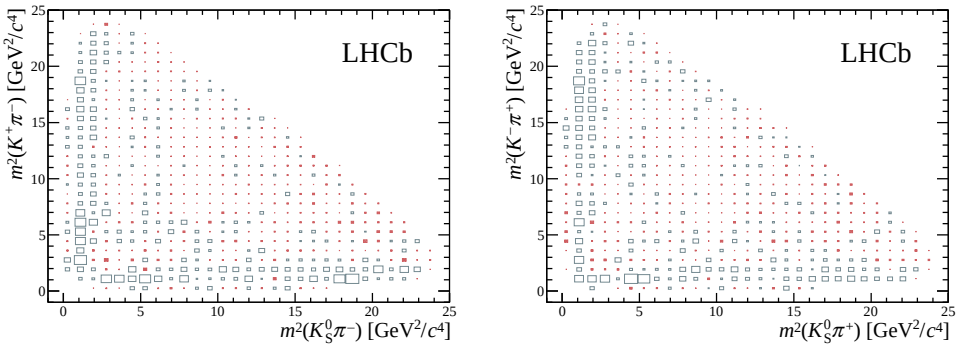

Fig. 2. – Dalitz plot distributions of the $K^0_S\ K^+\ \pi^-$ (left) and $K^0_S\ K^-\ \pi^+$ (right) final states. Crossed boxes designate negative values [8].

TABLE I. – *Fit fractions from the $B_s^0 \to K_S^0 K^\pm \pi^\mp$ baseline model fit and their statistical uncertainties.*

$K_S^0\ K^+\ \pi^-$		$K_S^0\ K^-\ \pi^+$	
Resonance	Fit fraction (%)	Resonance	Fit fraction (%)
$K^*(892)^-$	15.6 ± 1.5	$K^*(892)^+$	13.4 ± 2.0
$K_0^*(1430)^-$	30.2 ± 2.6	$K_0^*(1430)^+$	28.5 ± 3.6
$K_2^*(1430)^-$	2.9 ± 1.3	$K_2^*(1430)^+$	5.8 ± 1.9
$K^*(892)^0$	13.2 ± 2.4	$\overline{K}^*(892)^0$	19.2 ± 2.3
$K_0^*(1430)^0$	33.9 ± 2.9	$\overline{K}_0^*(1430)^0$	27.0 ± 4.1
$K_2^*(1430)^0$	5.9 ± 4.0	$\overline{K}_2^*(1430)^0$	7.7 ± 2.8

tures appear for $m^2(K_S^0 K^\pm)$. The baseline amplitude fit model is composed of resonant contributions from the $K^*(892)^{0,+}$, $K_0^*(1430)^{0,+}$, and $K_2^*(1430)^{0,+}$ and their conjugates. Vector and tensor states are described using relativistic Breit–Wigner functions, while the LASS lineshape [9], which combines the $K_0^*(1430)^0$ and a non-resonant component, is used to describe the scalar component. The baseline model fit results are shown in fig. 3, with the resulting fit fractions given in table I. The fit fractions are consistent for each resonance and its conjugate, hence no *CP*-violation effect is observed. Once systematic effects are accounted for, the contributions from $K_0^*(1430)$ states are observed with a significance of more than 10 Gaussian standard deviations.

Branching fraction products are obtained by converting the flavour-averaged fit fractions from the fit, using $\mathcal{B}(B_s^0 \to {}^{(}\overline{K}{}^{)0} K^\pm \pi^\mp) = (84.3 \pm 3.5 \pm 7.4 \pm 3.4) \times 10^{-6}$:

$$\begin{aligned}
\mathcal{B}(B_s^0 \to K^*(892)^\pm K^\mp; K^*(892)^\pm \to {}^{(}\overline{K}{}^{)0}\pi^\pm) &= \\
&(12.4 \pm 0.8 \pm 0.5 \pm \ \ 2.7 \pm 1.3) \times 10^{-6}\,, \\
\mathcal{B}(B_s^0 \to ({}^{(}\overline{K}{}^{)0}\pi^\pm)_0^* K^\mp) &= \\
&(24.9 \pm 1.8 \pm 0.5 \pm 20.0 \pm 2.6) \times 10^{-6}\,, \\
\mathcal{B}(B_s^0 \to K_2^*(1430)^\pm K^\mp; K_2^*(1430)^\pm \to {}^{(}\overline{K}{}^{)0}\pi^\pm) &= \\
&(\ \ 3.4 \pm 0.8 \pm 0.4 \pm \ \ 5.4 \pm 0.4) \times 10^{-6}\,, \\
\mathcal{B}(B_s^0 \to {}^{(}\overline{K}{}^{)*}(892)^0\ {}^{(}\overline{K}{}^{)0}; {}^{(}\overline{K}{}^{)*}(892)^0 \to K^\mp\pi^\pm) &= \\
&(13.2 \pm 1.9 \pm 0.8 \pm \ \ 2.9 \pm 1.4) \times 10^{-6}\,, \\
\mathcal{B}(B_s^0 \to (K^\mp\pi^\pm)_0^*\ {}^{(}\overline{K}{}^{)0}) &= \\
&(26.2 \pm 2.0 \pm 0.7 \pm \ \ 7.3 \pm 2.8) \times 10^{-6}\,, \\
\mathcal{B}(B_s^0 \to {}^{(}\overline{K}{}^{)}_2^*(1430)^0\ {}^{(}\overline{K}{}^{)0}; {}^{(}\overline{K}{}^{)}_2^*(1430)^0 \to K^\mp\pi^\pm) &= \\
&(\ \ 5.6 \pm 1.5 \pm 0.6 \pm \ \ 7.0 \pm 0.6) \times 10^{-6}\,,
\end{aligned}$$

where the $(K\pi)_0^*$ components refer to the total $K\pi$ S-wave and the quoted uncertainties are statistical, experimental and model systematic, and due to the uncertainty of $\mathcal{B}(B_s^0 \to {}^{(}\overline{K}{}^{)0} K^\pm \pi^\mp)$.

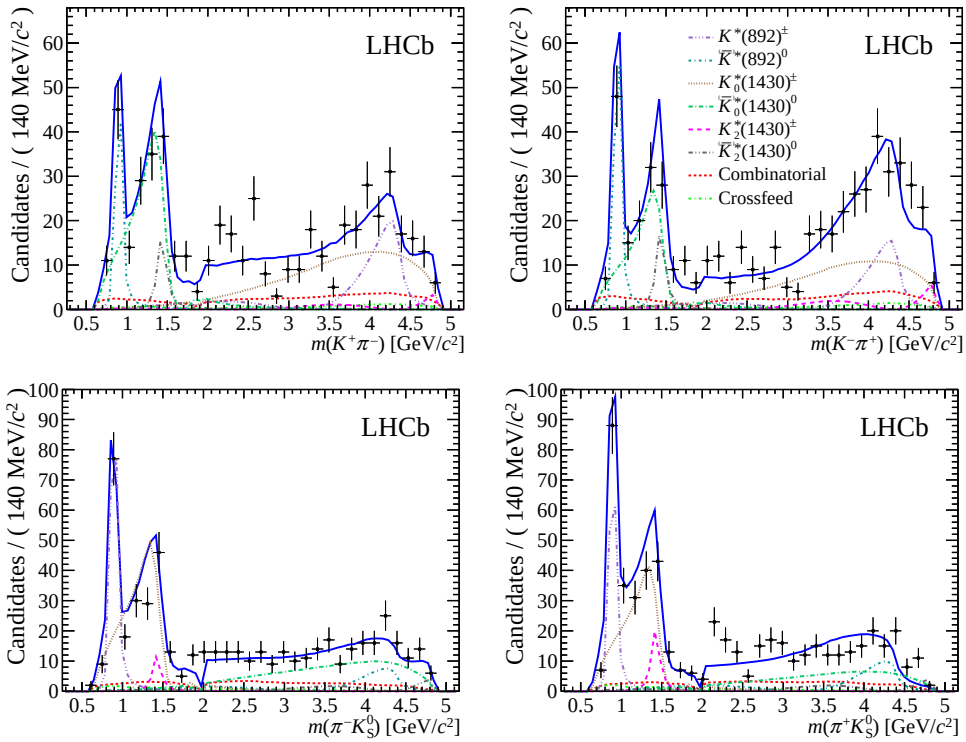

Fig. 3. – Two-body invariant mass distributions for $m(K^\pm\pi^-)$ (top) and $m(K^0_S\pi^\mp)$, and for the $K^0_S\ K^+\ \pi^-$ (left) and $K^0_S\ K^-\ \pi^+$ (right) final states [8].

3. – Amplitude analysis of $B^\pm \to \pi^\pm K^+ K^-$ decays

A previous study of the decay $B^\pm \to \pi^\pm K^+ K^-$ by the LHCb Collaboration observed very large *CP* asymmetries in specific regions of its phase space, in addition to a significant inclusive *CP* asymmetry [4]. The variation of $\mathcal{A}_{CP}$ across the phase phase was studied in bins of the Dalitz plot; a full amplitude analysis, the first for this particular decay, is presented here [10].

The event selection procedure is based on that of the previous analysis [4] and applied to the dataset taken by the LHCb detector in 2011 and 2012. PID is used to reduce backgrounds with misidentified kaons and pions, and a BDT is applied to remove combinatorial background. Candidates with two-body invariant mass lying within 30 MeV/c^2 of the known D^0 mass are vetoed to remove the contribution from intermediate charm decays.

The signal and background yields are determined using an unbinned extended maximum-likelihood fit performed simultaneously to both $B^+ \to \pi^+ K^+ K^-$ and $B^- \to \pi^- K^+ K^-$ invariant mass distributions. The amplitude analysis uses candidates in a restricted signal region, defined as $5266 < m(\pi^\pm K^+ K^-) < 5300\,\text{MeV}/c^2$. The signal yield in this region is 4865, of which 2052 are B^+ candidates and 1566 are B^- candidates. The DP distributions of the signal candidates can be seen in fig. 4.

In the binned $\mathcal{A}_{CP}$ analysis, the region above the $\phi(1020)$ resonance in the $K^+\ K^-$

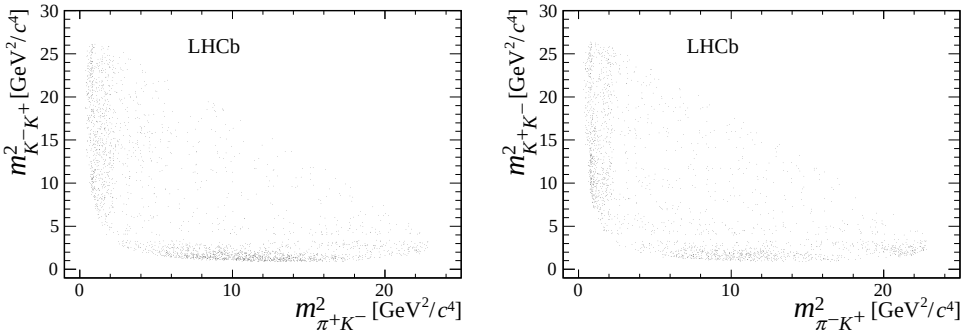

Fig. 4. – Dalitz plot distributions of the signal candidates in the $B^+ \to \pi^+K^+K^-$ (left) and $B^- \to \pi^-K^+K^-$ (right) final states [10].

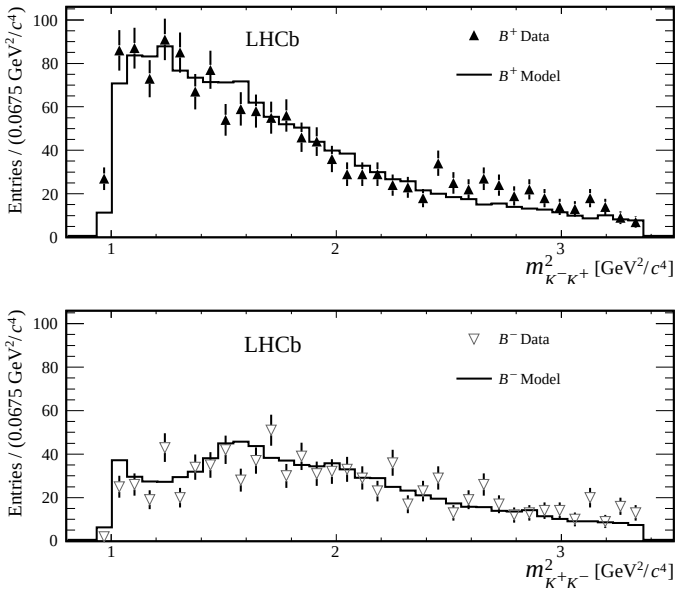

Fig. 5. – Distribution of the low-mass region in the m^2_{KK} system [10]. The projection of the fit result and data points are shown separated by charge.

two-body invariant mass spectrum was seen to exhibit very large negative $\mathcal{A}_{CP}$. However, no significant $B^\pm \to \phi\pi^\pm$ yield has previously been seen that could be associated with this effect [11]. One proposed explanation for the *CP* asymmetry in this region is the dynamic generation of *CP* violation via S-wave $\pi^+\pi^- \leftrightarrow K^+K^-$ scattering [12, 13]. A dedicated rescattering amplitude is included in the decay model, acting in the region $950 < m^2_{KK} < 1420\,\mathrm{MeV}/c^2$ and given by the off-diagonal term in the $\pi\pi - KK$ coupled-channel S-matrix [14].

The $K^+\,K^-$ system is further described by the inclusion of the $\rho(1450)^0$ and $f_2(1270)$ resonances. The two resonances are required to produce the destructive interference pattern seen at low m^2_{KK}, as shown in fig. 4. Furthermore, the $\phi(1020)$ resonance is

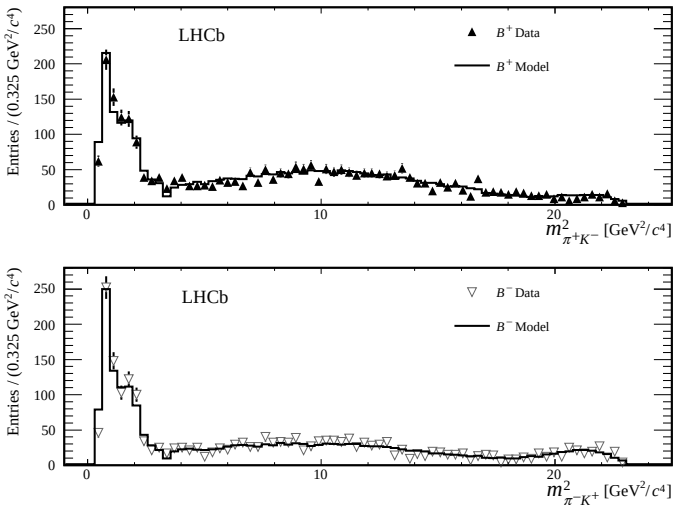

Fig. 6. – Distribution of the $m^2_{\pi K}$ system [10]. The projection of the fit result and data points are shown separated by charge.

included in the amplitude model, although its contribution is not established at high significance. The low-mass K^+ K^- region, with the result of the maximum-likelihood fit overlaid, is shown in fig. 5.

In the $\pi^\pm$ $K^\mp$ system, contributions from the $K^*(892)^0$ and $K^*_0(1430)^0$ resonances are included. Additionally, a non-resonant component described by a single-pole form factor is added to the model. This single-pole amplitude has the form [15]

$$F_R = \frac{1}{1 + m^2_{\pi K}/\Lambda^2}, \tag{2}$$

where Λ is an energy scale and is set to 1 GeV. The projection of the data and fit model onto $m^2_{\pi K}$ is shown in fig. 6.

The values of the fit fractions and *CP* asymmetries obtained from the fitted model are given in table II. The largest contribution comes from the single-pole non-resonant K π S-wave, closely followed by the $\rho(1450)^0$ component. The $\rho(1450)^0 \to K^+K^-$ fit fraction is larger than expected; the inclusion of the LHCb Run 2 dataset in a future analysis will help refine the knowledge of this region of the phase space. The rescattering amplitude has a significant fit fraction and a substantial $\mathcal{A}_{CP}$ value. It is the largest *CP* violation effect observed for any single amplitude.

4. – Conclusions

Recent results involving *CP* violation in multi-body charmless $B^\pm$ and B^0_s decays by the LHCb Collaboration have been presented in this document, specifically the amplitude analyses of $B^0_s \to K^0_S K^\pm \pi^\mp$ and $B^\pm \to \pi^\pm K^+ K^-$ decays. Other recent results, not reviewed here but also of note, include a measurement of *CP* asymmetries in charmless four-body b-baryon decays [16], and the amplitude analysis of $B^0 \to (\pi^+\pi^-)(K^+\pi^-)$ decays [17].

TABLE II. – *Fit fractions and CP asymmetries extracted from the result of the $B^\pm \to \pi^\pm K^+ K^-$ Dalitz plot fit. The first uncertainty is statistical and the second systematic.*

Contribution	Fit fraction (%)	$\mathcal{A}_{CP}$ (%)
$K^*(892)^0$	$7.5 \pm 0.6 \pm 0.5$	$+12.3 \pm 8.7 \pm 4.5$
$K_0^*(1430)^0$	$4.5 \pm 0.7 \pm 1.2$	$+10.4 \pm 14.9 \pm 8.8$
Single pole	$32.3 \pm 1.5 \pm 4.1$	$-10.7 \pm 5.3 \pm 3.5$
$\rho(1450)^0$	$30.7 \pm 1.2 \pm 0.9$	$-10.9 \pm 4.4 \pm 2.4$
$f_2(1270)$	$7.5 \pm 0.8 \pm 0.7$	$+26.7 \pm 10.2 \pm 4.8$
Rescattering	$16.4 \pm 0.8 \pm 1.0$	$-66.4 \pm 3.8 \pm 1.9$
$\phi(1020)$	$0.3 \pm 0.1 \pm 0.1$	$+9.8 \pm 43.6 \pm 26.6$

The untagged, decay-time-independent amplitude analysis of $B_s^0 \to K_S^0 K^\pm \pi^\mp$ has reported the observation of $K_0^*(1430)$ states with a significance above 10 standard deviations and updated the branching fractions of previously-measured quasi-two-body states. No significant *CP* violation is observed. Looking towards future analyses, a full tagged and decay-time-dependent amplitude analysis of this decay will be possible with the much larger dataset expected after future LHCb upgrades.

The first amplitude analysis of the $B^\pm \to \pi^\pm K^+ K^-$ decay has identified seven components in the decay amplitude of this decay, with the largest contributions originating from $K\,\pi$ non-resonant S-wave and the $\rho(1450)^0$ resonance. A dedicated $\pi^+\pi^- \leftrightarrow K^+K^-$ rescattering amplitude is found to generate a *CP* asymmetry of $(-66 \pm 4 \pm 2)\%$, the largest effect observed for a single amplitude to date.

* * *

The author wishes to thank the organisers of the Rencontres de Physique de la Vallée d'Aoste for providing the opportunity to present these results.

REFERENCES

[1] CABIBBO N., *Phys. Rev. Lett.*, **10** (1963) 531.
[2] KOBAYASHI M. and MASKAWA T., *Prog. Theor. Phys.*, **49** (1973) 652.
[3] AAIJ R. *et al.*, *Phys. Rev. D*, **98** (2018) 032004.
[4] AAIJ R. *et al.*, *Phys. Rev. D*, **90** (2014) 112004.
[5] AAIJ R. *et al.*, *JHEP*, **03** (2018) 140.
[6] AAIJ R. *et al.*, *JHEP*, **10** (2013) 143.
[7] AAIJ R. *et al.*, *JHEP*, **11** (2017) 027.
[8] AAIJ R. *et al.*, *JHEP*, **06** (2019) 114.
[9] ASTON D. *et al.*, *Nucl. Phys. B*, **296** (1988) 493.
[10] AAIJ R. *et al.*, arXiv:1905.09244.
[11] AAIJ R. *et al.*, *Phys. Lett. B*, **728** (2014) 85.
[12] WOLFENSTEIN L., *Phys. Rev. D*, **43** (1991) 151.
[13] BIGI., I. I. and SANDA, A. I., *CP violation*, *Camb. Monogr. Part. Phys. Nucl. Phys. Cosmol.*, **9** (2009) 1.
[14] PELAEZ J. R. and YNDURAIN, F. J., *Phys. Rev. D*, **71** (2005) 074016.
[15] ALVARENGA NOGUEIRA J. H. *et al.*, *Phys. Rev. D*, **92** (2015) 054010.
[16] AAIJ R. *et al.*, arXiv:1903.06792.
[17] AAIJ R. *et al.*, *JHEP*, **05** (2019) 026.